Check for updates

Geophysical Research Letters

RESEARCH LETTER
10.1029/2022GL099250

A Minimally Cemented Shallow Crust Beneath InSight

Vashan Wright[1], Jhardel Dasent[1], Richard Kilburn[1], and Michael Manga[2]

[1]University of California San Diego, Scripps Institution of Oceanography, La Jolla, CA, USA, [2]Department of Earth and Planetary Science, University of California Berkeley, Berkeley, CA, USA

Key Points:

- Any significant volumes of ice or mineral cements within the upper 300 m beneath InSight are likely nodular or broken
- No ice- or liquid water-saturated layers were seismically resolved within the upper 300 m beneath InSight
- Up to 20% ice is permissible within the pores of fractured basalt layers in the upper 300 m beneath InSight

Supporting Information:

Supporting Information may be found in the online version of this article.

Correspondence to:

V. Wright,
vwright@ucsd.edu

Citation:

Wright, V., Dasent, J., Kilburn, R., & Manga, M. (2022). A minimally cemented shallow crust beneath InSight. *Geophysical Research Letters*, *49*, e2022GL099250. https://doi.org/10.1029/2022GL099250

Received 22 APR 2022
Accepted 29 JUL 2022

Author Contributions:

Conceptualization: Michael Manga
Data curation: Jhardel Dasent
Formal analysis: Jhardel Dasent, Richard Kilburn
Funding acquisition: Michael Manga
Investigation: Richard Kilburn
Methodology: Jhardel Dasent, Richard Kilburn, Michael Manga
Supervision: Michael Manga
Visualization: Jhardel Dasent
Writing – review & editing: Jhardel Dasent, Richard Kilburn, Michael Manga

© 2022. American Geophysical Union. All Rights Reserved.

Abstract Ice and other mineral cements in Mars' shallow subsurface affect the mechanical properties of the shallow crust, the geologic processes that shape the planet's surface, and the search for past or extant Martian life. Cements increase seismic velocities. We use rock physics models to infer cement properties from seismic velocities. Model results confirm that the upper 300 m of Mars beneath InSight is most likely composed of sediments and fractured basalts. Grains within sediment layers are unlikely to be cemented by ice or other mineral cements. Hence, any existing cements are nodular or formed away from grain contacts. Fractures within the basalt layers could be filled with gas, 2% mineral cement and 98% gas, and no more than 20% ice. Thus, no ice- or liquid water-saturated layers likely exist within the upper 300 m beneath InSight. Any past cement at grain contacts has likely been broken by impacts or marsquakes.

Plain Language Summary Quantifying how much and where ice and other minerals exist within Mar's shallow subsurface may help to determine if Mars ever supported life, to understand its climate history, to understand Mars as a geological system, and to prepare for human exploration. The InSight lander on Mars has an instrument whose data provide estimates for the velocity of seismic waves within the crust. These velocities change depending on rock type and the material that fills the pores within rocks. Possible pore-filling materials include gas, liquid water, ice, and other mineral cements. We find that the shallow crust is at best weakly cemented and the pores within the rocks are not entirely filled with ice or liquid water.

1. Introduction

Cements in the Martian crust can have multiple origins, including ice frozen from liquid water or condensed from vapor, hydrated minerals formed in situ, or minerals precipitated from aqueous fluids (e.g., salts, carbonates, and sulfates). The presence, amount, and composition of ice and other mineral cements in the shallowest sections of the Martian crust have implications for robotic and human exploration of Mars, the processes that shape and shaped the surface, and the search for past or extant life. Research on these topics is central to determining if Mars ever supported life, to understand the climate history and processes, to understand Mars as a geological system, and to prepare for human exploration.

Cementation affects and records geological processes. Cement can strengthen sediments (herein defined to include regolith and all other granular media layers) by creating stiffer contacts between particles. Cementation affects the permeability and porosity of sediments and fractured rocks, which impacts gas transport driven by atmospheric pressure changes (Morgan et al., 2021). Pores and fractures filled with ice or other mineral cement could confine any deeper liquid water, creating aquifers (Carr, 1979). Ground ice can promote weak explosive eruptions at rootless cones on lava flows (Brož et al., 2021) and may promote phreatomagmatic eruptions (Moitra et al., 2021). Cemented sediments are less prone to eolian and fluvial transport and erosion. The distribution of cements in the Martian sediments may record the accumulation and transport of volatiles in geologically recent times (Dundas et al., 2021). Cements may also preserve organic compounds diagnostic of past or present biological activity (Rivera-Valentín et al., 2020).

Cementation impacts human exploration, and a primary motivation for the Mars Ice Mapper mission concept is to map ice in the shallowest crust (Davis & Haltigin, 2021). The presence of ice and hydrated minerals in shallow sediments and fractured rocks could provide a source of water for in situ resource utilization (Piqueux et al., 2019). Cementation-induced strengthening of sediments affects foundations used for engineering infrastructure (Kalapodis et al., 2020). Cemented sediments can be used as a construction material (Liu et al., 2021) and have prompted studies of a range of Mars simulants in preparation for future human missions (Karl et al., 2021).

19448007, 2022, 15, Downloaded from https://agupubs.onlinelibrary.wiley.com/doi/10.1029/2022GL099250 by University Of California, Wiley Online Library on [18/04/2025]. See the Terms and Conditions (https://onlinelibrary.wiley.com/terms-and-conditions) on Wiley Online Library for rules of use; OA articles are governed by the applicable Creative Commons License

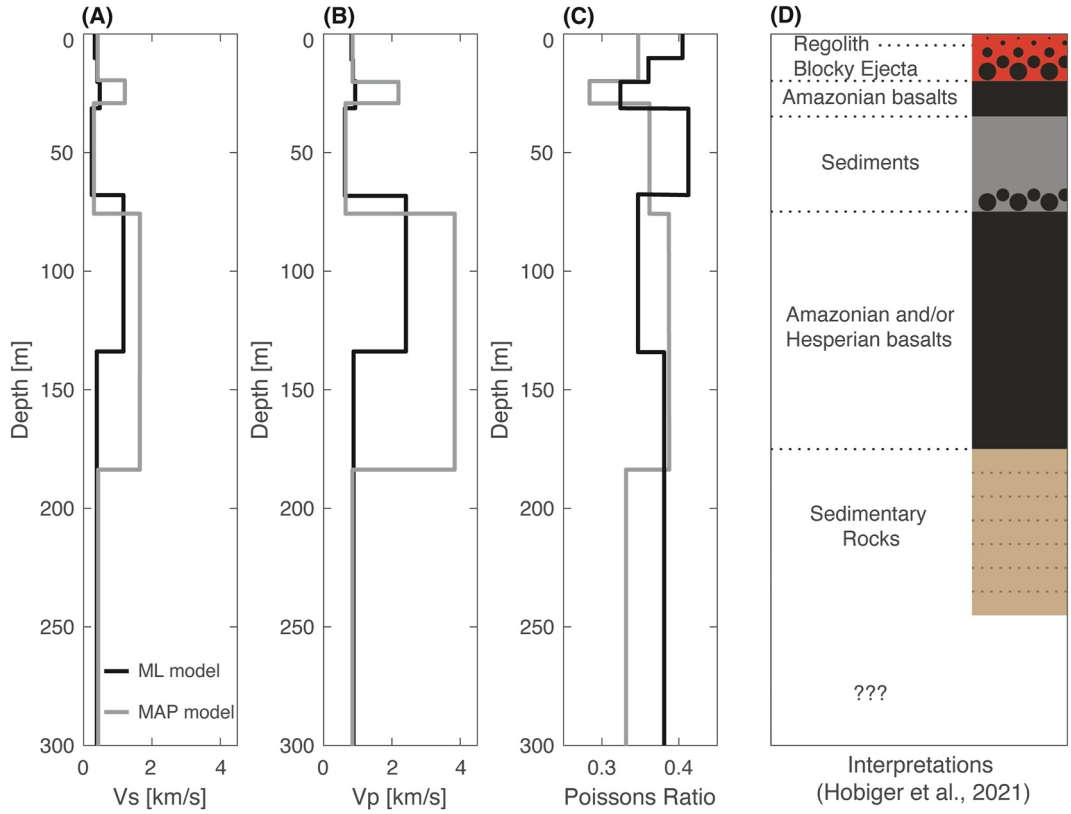

Figure 1. Models of (a) V_s and (b) V_p from Hobiger et al. (2021) and (c) calculated Poisson's ratio based on the seismic velocities. The black and gray curves are Hobiger et al. (2021)'s maximum likelihood and maximum a posteriori models, respectively (d) Inferred stratigraphy of the upper 300 m beneath InSight, from Hobiger et al. (2021).

Efforts to map and study shallow subsurface ice and other mineral cements integrate complementary insights from direct and indirect observations. Direct, in situ measurements of ice and other mineral cements at specific landing sites are possible, yet sometimes challenging. The Phoenix lander excavated ice in the upper few cm (Morgan et al., 2021). Eolian processes and impact brecciation created a 10–30 m thick regolith (including a sand horizon in the upper 3 m) at the InSight (Interior Exploration using Seismic Investigations, Geodesy, and Heat Transport mission) landing site (Golombek et al., 2020; Warner et al., 2022). There, the rover had difficulties penetrating its heat flow probe into the subsurface owing to insufficient friction (Spohn et al., 2022). Indirect methods of detecting ice and other mineral cements include analyses of neutron detection, thermal inertia, geomorphic, and radar data (Morgan et al., 2021). Other indirect methods exploit the sensitivity of geomechanical properties to cements, which influence geophysical properties such as seismic velocity, electrical conductivity, and gravity. For example, Manga and Wright (2021) used seismic velocities interpreted with rock physics models for fractured rocks to infer that there is likely no ice-saturated cryosphere in the 0–7.5 km depth range beneath the InSight landing site, though they suggested that some mineral cement could be present at greater depths.

Here we study the presence and quantity of mineral and ice cements in the upper 300 m of the Martian crust by interpreting seismic velocity models derived from data collected by the seismometer deployed by the InSight lander. We interpret the seismic velocities using rock physics models for both fractured rocks and sediments. We also interpret seismic velocities using a theoretical relationship between dry-frame Poisson's ratio and grain contact forces in sediments. Figure 1 based on results from Hobiger et al. (2021) shows their derived seismic velocities beneath InSight and the inferred stratigraphy and lithology. Shear wave velocities V_s generally increase from ~0.3 km/s at the surface to ~1.7 km/s at 175 m; compressional wave velocities V_p increase from ~0.8 km/s to ~3.8 km/s within the same depth. At least two low velocity zones exist from 0 to 157 m and 175–300 m, where V_s decreases to ~0.4 km/s and V_p decreases to ~0.8–0.9 km/s Hobiger et al. (2021) interpreted the higher and lower velocity layers as fractured basalts and sediment, respectively (Figure 1d), consistent with geological mapping (Warner et al., 2022). Our interpretations of these seismic velocities are that sediments within the upper

19448007, 2022, 15, Downloaded from https://agupubs.onlinelibrary.wiley.com/doi/10.1029/2022GL099250 by University Of California, Wiley Online Library on [18/04/2025]. See the Terms and Conditions (https://onlinelibrary.wiley.com/terms-and-conditions) on Wiley Online Library for rules of use; OA articles are governed by the applicable Creative Commons License

300 m of the Martian crust are gas-filled; mineral or ice cements likely do not exist at grain contacts and there is no evidence for any ice-saturated cryosphere.

2. Methods

2.1. Inferring Subsurface Properties Using Rock Physics Models

We compare measured with theoretically modeled V_s and V_p to infer the mechanical properties of the upper 300 m beneath Insight, constraining uncertainties with Monte Carlo analyses. For sediments, we assume a porosity reduction profile for Mars, predict seismic velocities with that assumed profile, then compare modeled to measured velocities within the lower velocity zones. For fractured basalt layers, we create rock physics templates that relate seismic velocities, porosity ϕ (0%–50%), and fracture shape represented by elliptical inclusions with an aspect ratio, defined as the short axis divided by long axis, $\alpha = 0.01$–1. We use the templates to identify the combinations of porosity and fracture shapes that could explain both measured V_p and V_s within the higher velocity zones.

We compute V_s and V_p from

$$V_s = \sqrt{\frac{\mu_e}{\rho}} \tag{1}$$

$$V_p = \sqrt{\frac{\kappa_e + \frac{4}{3}\mu_e}{\rho}} \tag{2}$$

where ρ, κ_e, and μ_e are bulk density, effective bulk modulus, and effective shear modulus, respectively. Bulk density ρ is

$$\rho = \sum_i \phi_i \rho_i \tag{3}$$

where ρ_i and ϕ_i are densities and volume fractions of the ith constituents, respectively.

Rock physics theoretical models predict dry-frame shear and bulk moduli (μ and κ); $\mu_e = \mu$ and $\kappa_e = \kappa$ for dry rock (Biot, 1956; Gassmann, 1951). We use Hertz-Mindlin's (Mindlin, 1949) rock physics models for uncemented sediments. We use the contact cement model (Dvorkin & Nur, 1996) for sediments with cement that completely surrounds grains that are in contact or cement that only exists at grain contacts. We use the Berryman self-consistent model (Berryman, 1980) for fractured rocks. The equations for the rock physics models are in Mindlin (1949), Dvorkin and Nur (1996), and Berryman (1980).

We use Gassmann-Biot fluid substitution theory (Biot, 1956; Gassmann, 1951) to calculate effects of fluid saturation on κ (i.e., κ_e for liquid water saturated rocks),

$$\frac{\kappa_e}{\kappa_m - \kappa_e} - \frac{\kappa_{f2}}{\phi(\kappa_m - \kappa_{f2})} = \frac{\kappa}{\kappa_m - \kappa} + \frac{\kappa_{f1}}{\phi(\kappa_m - \kappa_{f1})} \tag{4}$$

where κ_{f_2}, κ_m, and κ_{f1} are the bulk moduli of the saturating fluid (liquid water in our case), mineral(s), and gas (0 kPa), respectively. Gassmann-Biot theory assumes that fluids are not flowing and minerals and fluids homogeneously distribute within rocks (Biot, 1956; Gassmann, 1951).

The models' input parameters are porosity ϕ, coordination number c_n (average number of grains in contact), effective pressure P, mineral Poisson's ratio ν_m, cement fraction c_f, mineral bulk κ_m and shear μ_m moduli, pore aspect ratio α, and grain roughness fraction f (i.e., percentage of grain contacts that allows tangential slip, which we assume to be 0% or 100% to model end-member ranges). We assume porosity ϕ at the surface (critical porosity ϕ_c) is between 0.3 and 0.5 (Golombek et al., 2018; Lewis et al., 2019; Lognonné et al., 2020; Smrekar et al., 2019) and that ϕ exponentially decays with depth z,

$$\phi = \phi_c e^{-\frac{z}{k}} \tag{5}$$

19448007, 2022, 15, Downloaded from https://agupubs.onlinelibrary.wiley.com/doi/10.1029/2022GL099250 by University Of California, Wiley Online Library on [18/04/2025]. See the Terms and Conditions (https://onlinelibrary.wiley.com/terms-and-conditions) on Wiley Online Library for rules of use; OA articles are governed by the applicable Creative Commons License

where k is a compaction constant (2.82 km) scaled to Mars' gravitational field (Clifford, 1986). Effective pressure P is

$$P = \rho g h - p_f \tag{6}$$

where g, h, and p_f represent Mars' gravitational acceleration (3.71 m/s^2), depth, and fluid pressure, respectively. We constrain coordination number c_n empirically (Murphy, 1982)

$$c_n = 20 - 34\phi + 14\phi^2. \tag{7}$$

The minerals that we use in the models and their respective κ_m and μ_m in GPa are calcite cement (71.6 and 28.2), basalt grains and rocks (80.0 and 40.0), and ice cement (8.7 and 3.8) (Vanorio et al., 2003; Zong et al., 2017). These are some of the main minerals expected within the upper 300 m of the Martian crust (Golombek et al., 2018; Pan et al., 2020; Tanaka et al., 2014); we also consider other cements listed in Table S1 in Supporting Information S1. We calculate mineral Poisson's ratio from

$$\nu_m = \frac{3\kappa_m - 2\mu_m}{6\kappa_m + 2\mu_m}. \tag{8}$$

We use Monte Carlo analyses to constrain the effects of input parameter uncertainties on the velocities predicted by the rock physics model for cemented and uncemented sediments. In each of our 10,000 realizations, we randomly generate and use a new input parameter value between their ranges. We generate new ϕ-depth profiles from the selected ϕ_c. Coordination numbers, bulk densities, and effective pressures change with ϕ-depth profiles.

2.2. Inferring Subsurface Properties From Poisson's Ratio

We infer the volume fraction of cemented grain contacts from the relationship between Poisson's ratio ν_d and f, the volume fraction of rough versus smooth grain contacts. Rough (smooth) grain contacts resist (allow) elastic tangential grain contact slip during seismic wave propagation. We conjecture that, in the absence of cemented grains, Martian sediments comprise nearly 100% smooth grain contacts. We make this conjecture because Mars' gravitational acceleration (3.7 m/s^2) is lower than Earth's (9.8 m/s^2). Gravitational acceleration impacts grain contact forces significantly (Equation 6). Assuming 100% smooth grain contacts routinely results in better seismic velocities predictions in shallow sediments on Earth (up to 600 m below the surface in some cases) (Buckingham, 2000; Majmudar & Behringer, 2005; Wright & Hornbach, 2021; Zimmer et al., 2007). Low friction at grain contacts, despite cohesion and possibly partial cementation, appears to have prevented InSight's heatflow probe from penetrating the shallow subsurface (Spohn et al., 2022). Given the assumptions, conjectures, and expectations mentioned, cements are likely one of the main causes for rough grain contacts, making f synonymous with the volume of cemented grain contacts in those cases. We compute f from ν_m and ν_d for an aggregate of identical perfect spheres (Bachrach & Avseth, 2008; Walton, 1987)

$$\nu_d = \frac{(2 - \nu_m)}{4\,(2 - \nu_m) + 2f\,(1 - \nu_m)} - \frac{2f\,(1 - \nu_m)}{4\,(2 - \nu_m) + 2f\,(1 - \nu_m)}. \tag{9}$$

f decreases as ν_d increases (Walton, 1987). We compute ν_d from the measured V_p and V_s

$$\nu_d = \frac{1}{2}\frac{(V_p/V_s)^2 - 2}{(V_p/V_s)^2 - 1}. \tag{10}$$

Our calculation assumes that there is no liquid water within the sediment layers.

3. Results

3.1. Inferred Pore-Filling Media in Sediments

The sediment layers most likely host grains that experience relatively low friction at contacts. Low friction is indicated by the observation that smooth-grained models produce better seismic velocity predictions (i.e., lower misfits) than rough-grained models, regardless of assumed pore-filling material (Figure 2). The differences between smooth-versus rough-grain model predictions are 0.3–0.4 km/s and 0.1–0.5 km/s for V_s and V_p, respectively. Low friction is also indicated by the Poisson's ratio for sediment layers, 0.33–0.41 (Figure 1). These

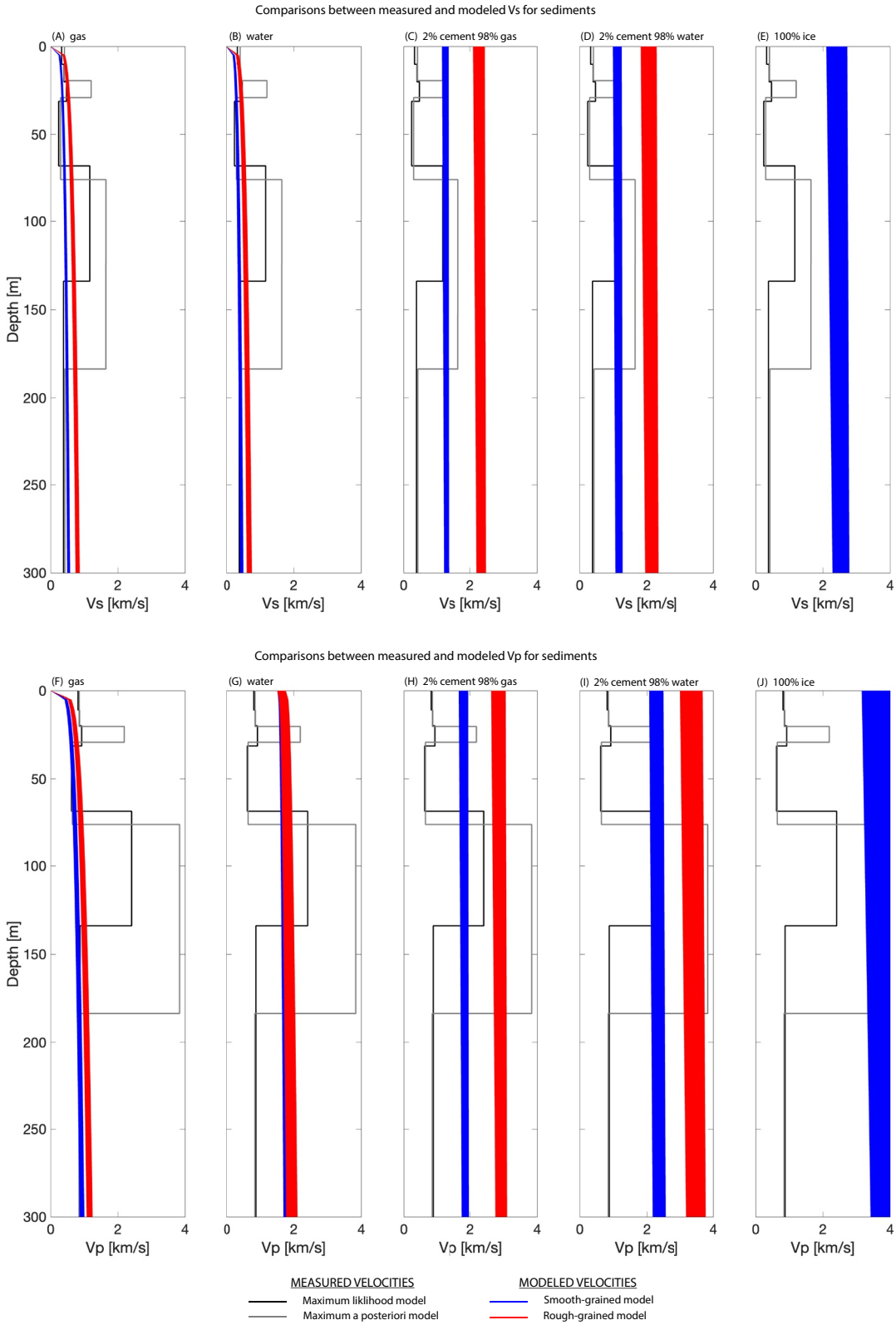

Figure 2. Measured V_p and V_s (black and gray lines) compared to model predicted V_p and V_s for sediment whose pores are filled with gas, liquid water, 2% calcite cement and 98% gas, 2% calcite cement and 98% liquid water, and ice. Blue and red lines are the smooth-grained and rough-grained model results, respectively.

19448007, 2022, 15, Downloaded from https://agupubs.onlinelibrary.wiley.com/doi/10.1029/2022GL099250 by University Of California, Wiley Online Library on [18/04/2025]. See the Terms and Conditions (https://onlinelibrary.wiley.com/terms-and-conditions) on Wiley Online Library for rules of use; OA articles are governed by the applicable Creative Commons License

19448007, 2022, 15, Downloaded from https://agupubs.onlinelibrary.wiley.com/doi/10.1029/2022GL099250 by University Of California, Wiley Online Library on [18/04/2025]. See the Terms and Conditions (https://onlinelibrary.wiley.com/terms-and-conditions) on Wiley Online Library for rules of use; OA articles are governed by the applicable Creative Commons License

Poisson's ratio values result in negative values (−0.55 to −0.10) for the calculated volume fraction of rough grains (Equation 10), which indicates that there are likely no rough grain contacts present, that the model breaks down for such high values, or both.

The pores within the sediment layers are most likely filled with gas (Figure 2). Modeled smooth-grained V_s for gas and liquid water-filled pores are within 0–0.1 km/s of measured V_s. Modeled V_p are within 0.01–0.05 km/s of measured V_p, assuming that gas fills the pores; assuming 100% liquid water in the pores results in V_p overprediction by 0.6–1.0 km/s. Models that assume pores are filled with 2% cement overpredict V_p and V_s by 1.4–3.0 km/s. Assuming that ice fills the pores results in V_p and V_s overpredictions by 2.3–3.2 km/s and 1.7–2.4 km/s, respectively for the sediments.

3.2. Inferred Pore-Filling Media in Fractured Basalts

The hypothesized fractured basalt layers could host 100% gas, 100% liquid water, 2% calcite cement and 98% air, or 2% calcite cement and 98% water in the fractures (Figure 3); hosting 100% ice is unlikely (Figure 4). A gas-filled basalt requires the narrowest range of aspect ratio and porosity combination to be consistent with the measured seismic velocities. A liquid water-filled basalt is consistent with the measured seismic velocities if the basalts' porosities are between 0.13 and 0.47 for aspect ratios between 0.03 and 1; aspect ratios increase with increasing porosities. A basalt hosting 2% calcite cement and 98% gas or liquid water in its fractures could explain the measured velocities if the porosities are 0.24–0.5. The range of possible aspect ratios increases with increasing porosities. All combinations of porosities and aspect ratios for a 100% ice-filled basalt results in velocities that are 1.1–2.8 times higher than measured. Thus, measured V_s and V_p are too low for a 100% ice-filled fractured basalt.

4. Discussion

We now discuss our most robust interpretations for the distribution of cements within the upper 300 m beneath InSight, considering the model assumptions and limitations. The cemented and uncemented granular media models assume that grains are identical spheres experiencing equal contact forces, which are idealizations for Martian and other sediments (Bachrach & Avseth, 2008; Day-Lewis et al., 2005; Majmudar & Behringer, 2005; Makse et al., 1999, 2004). These model assumptions sometimes lead to overpredictions in low effective stress environments on Earth (Buckingham, 2000; Majmudar & Behringer, 2005; Wright & Hornbach, 2021; Zimmer et al., 2007). The cementation models predict elastic moduli by homogeneously distributing the entire volume of cement within the sediments, which may also be too idealistic for actual sediments (Dvorkin & Nur, 1996). Considering the model limitations, we can still make two main interpretations: any shallow cements in Martian sediments likely do not adhere grains, and pores within the layers are not filled with liquid water or ice.

4.1. Fractured Basalt Layers With up to 20% of Its Pores Filled With Ice

A seismically detectable cryosphere likely does not exist within the upper 300 m beneath InSight. This is indicated by the observation that the granular and fractured media models predict velocities that are too high for fully ice-saturated sediments and basalt. Manga and Wright (2021) drew a similar conclusion for the upper 8 km of crust because their modeled V_s for an ice-saturated basalt was high compared to measured V_s. It is unlikely that we misinterpreted a basalt layer for an ice-saturated sediment layer; the predicted V_p for the Amazonian and/or Hesperian basalt layer matches, but V_s is overpredicted by at least 0.5–2.3 km/s (Figures 1 and 2). A partial cryosphere, with up to 20% ice, could exist in the fractured basalt layers. Though the measured velocities are consistent with modeled velocities for a fractured basalt whose pores are filled with up to 40% ice, porosities of basaltic lava flows rarely reach such high values except in thin horizons where vesicles accumulate (Cashman & Kauahikaua, 1997) or when chemical reactions alter the minerals within the basalt and lead to higher porosities (Broglia & Ellis, 1990; Franzson et al., 2010). Moreover, estimated and modeled porosity for exposed Martian basalts and meteorites are less than 40% (Hanna & Phillips, 2005; MacKinnon & Tanaka, 1989). Limiting the range of porosity to up to 40% then implies that measured velocities are only consistent with a basalt with less than 20% of the pores filled with ice. We did not model the effects of salinity on ice and seismic velocities; increased salinity may lead to mushy ice in the pores and reduce seismic velocities, depending on the

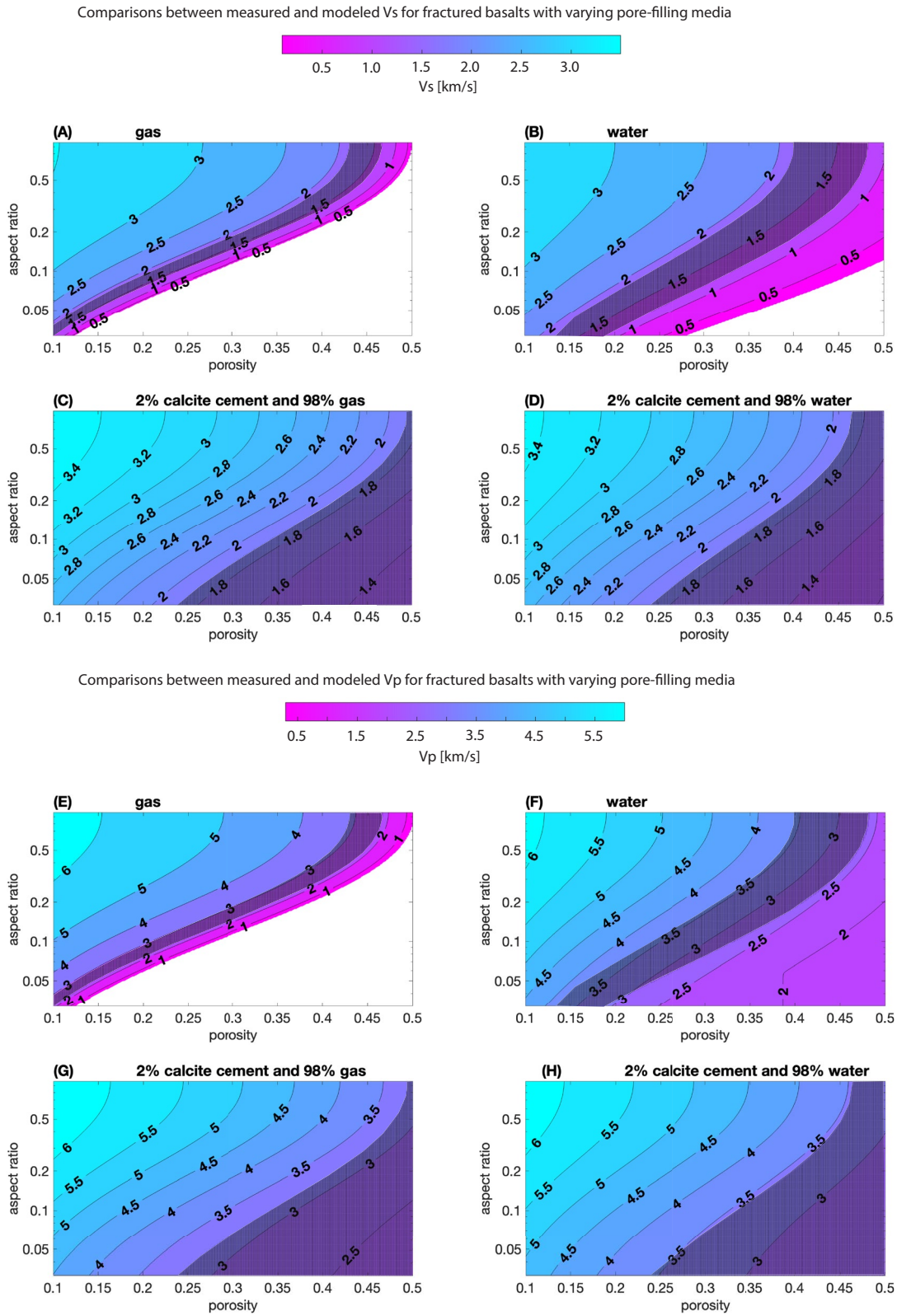

Figure 3. Rock physics model templates showing predicted V_s and V_p for a fractured basalt with various pore-filling materials. Shaded regions are the combinations of modeled velocities, porosities, and aspect ratios that match both the measured V_p and V_s for the higher velocity zones. Vertical scale is logarithmic.

19448007, 2022, 15, Downloaded from https://agupubs.onlinelibrary.wiley.com/doi/10.1029/2022GL099250 by University Of California, Wiley Online Library on [18/04/2025]. See the Terms and Conditions (https://onlinelibrary.wiley.com/terms-and-conditions) on Wiley Online Library for rules of use; OA articles are governed by the applicable Creative Commons License

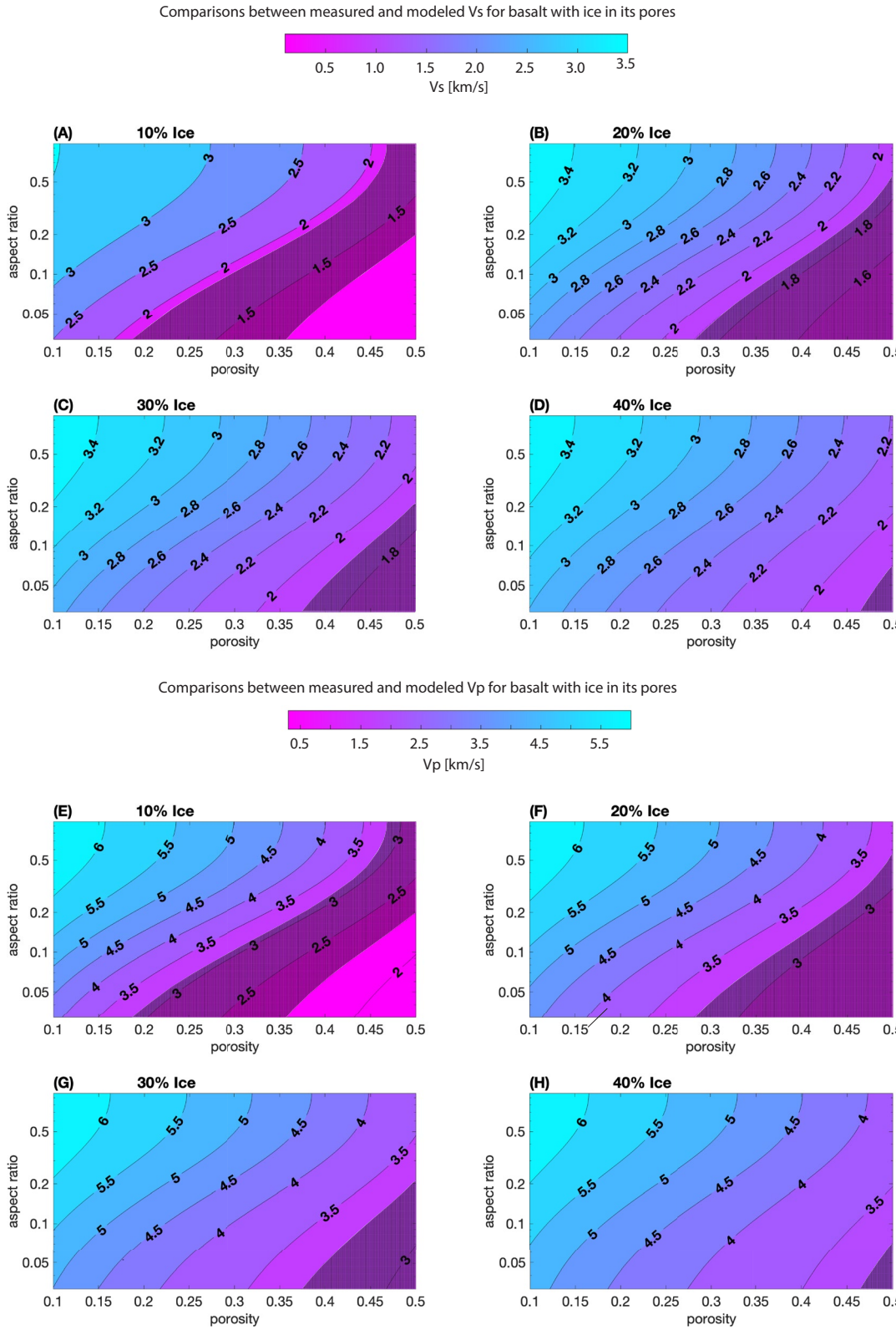

Figure 4. (a–h) Rock physics model templates showing predicted V_s and V_p for a fractured basalt with varying percentages of ice within the fractures. Shaded regions are the combinations of modeled velocities, porosities, and aspect ratios that match both measured V_s and V_p from Hobiger et al. (2021). Vertical scale is logarithmic. Figure S2 in Supporting Information S1 contains rock physics model templates showing predicted V_s and V_p for a basalt whose fractures are 50% and 100% filled with ice.

19448007, 2022, 15, Downloaded from https://agupubs.onlinelibrary.wiley.com/doi/10.1029/2022GL099250 by University Of California, Wiley Online Library on [18/04/2025]. See the Terms and Conditions (https://onlinelibrary.wiley.com/terms-and-conditions) on Wiley Online Library for rules of use; OA articles are governed by the applicable Creative Commons License

temperatures and wetting behavior (Dou et al., 2017). We also did not consider crustal V_s anisotropy, which may be used to constrain the orientation of cracks (Li et al., 2022). Future studies could explore these possibilities.

Our inferences are consistent with findings from the Mars Subsurface Water Ice Mapping (SWIM) project, which used neutron detection, thermal inertia, geomorphology, radar surface mapping, and radar dielectric analysis to search for shallow subsurface ice (Morgan et al., 2021). The SWIM data compilation suggests that shallow ice is unlikely to be present at the near-equatorial landing site of InSight, 4.5°N. SWIM is most sensitive to the upper few meters, though radar reflection can probe depths greater than 100 m. Our finding that the shallowest sediment layer, which extends to 20–70 m, likely does not contain ice that cements grains is consistent with the SWIM map.

4.2. Mineral Cements as Framework Grains in Sediment Layers

Most mineral cements, if they exist, likely do not adhere grains substantially. Support for this interpretation comes from the observation that there are likely no significant volumes of rough grain contacts in sediments, as indicated by the high Poisson's ratios. Additional support comes from the observation that the models with calcite cement at grain contacts and surrounding the grains overpredict V_p and V_s by 1.4–3.0 km/s. Other mineral cements (e.g., halite, ice, gypsum, or kaolinite) also likely do not adhere grains since the differences in the elastic moduli between calcite and other mineral cements would not lead to a 1.4–3.0 km/s increase in seismic velocities (Figure S1 in Supporting Information S1). Nodular cements and concretions that are a part of the network of framework grains or cements that form on grains without adhering to other grains could exist. These cement types would produce roughly the same seismic velocities as gas-filled sediment with the same porosity. Thus, any existing cements likely resulted from mineral alteration, such as hydrating minerals (Scheller et al., 2021; Wernicke & Jakosky, 2021), precipitating salts (Sun et al., 2019), or the formation of concretions or spherules (Squyres et al., 2004, 2006).

Cements could have formed at the grain contacts of Martian sediments, only to be later broken by impacts and strong marsquakes. For example, the impacts that formed the large Noachian basins create dynamic strains similar to magnitude 10 and 11 quakes and could disrupt sediment globally on Mars (Clifford, 1997; Wang et al., 2005). Strains from smaller, local impacts and impact gardening of the surface might also disrupt cements in the younger Amazonian and Hesperian sediments and basalts in the upper few hundred meters. Laboratory experiments show that, depending on the porosity of the sediments and degree of cementation (weakly or strongly cemented), the relatively low strain rates from cyclic shearing (i.e., the type of waves experienced during seismic events) can break weekly cemented bonds (Sharma & Fahey, 2003; Suazo et al., 2017; Suzuki et al., 2012; Zeghal & El Shamy, 2008).

5. Conclusions

The presence, volume, and distribution of ice and other mineral cements in Martian sediments and fractured rocks may record and affect geologic processes. Seismic velocities are sensitive to cement properties, and rock physics models provide one approach to relate cement properties to seismic velocities. Using these models to interpret seismic velocities derived from InSight data, we find that any cement within the upper 300 m beneath InSight likely does not cement grain contacts in sediments. An ice-saturated sediment or fractured basalt layer likely does not exist, but fractured basalts whose pores contain up to 20% ice are possible. The findings support the ideas that some of Mars' past surface liquid water could be incorporated in cements that resulted from mineral alteration, precipitating salts, or the formation of concretions or spherules. Any cement at grain contacts was likely either weak and perhaps broken by impacts or marsquakes. Future studies could revisit these inferences as more constraints become available on the porosity, mineralogy, lithology, density, seismic velocity, and heat flow within the shallowest sections of the Martian crust.

Data Availability Statement

No new data was used in this study. The seismic velocity models are available in Hobiger et al. (2021).

19448007, 2022, 15, Downloaded from https://agupubs.onlinelibrary.wiley.com/doi/10.1029/2022GL099250 by University Of California, Wiley Online Library on [18/04/2025]. See the Terms and Conditions (https://onlinelibrary.wiley.com/terms-and-conditions) on Wiley Online Library for rules of use; OA articles are governed by the applicable Creative Commons License

Acknowledgments
Thanks to NASA and the InSight team for their vision, hard work, and dedication, especially during this time when COVID-19 is real. V. Wright, J. Dasent, and R. Kilburn acknowledge support from NSF grant 2136301. M. Manga acknowledges support from NASA Grant 80NSSC19K0545 and the CIFAR Earth 4D program.

References

Bachrach, R., & Avseth, P. (2008). Rock physics modeling of unconsolidated sands: Accounting for nonuniform contacts and heterogeneous stress fields in the effective media approximation with applications to hydrocarbon exploration. *Geophysics*, *73*(6), E197–E209. https://doi.org/10.1190/1.2985821

Berryman, J. G. (1980). Long-wavelength propagation in composite elastic media II. Ellipsoidal inclusions. *Journal of the Acoustical Society of America*, *68*(6), 1820–1831. https://doi.org/10.1121/1.385172

Biot, M. A. (1956). Theory of propagation of elastic waves in a fluid-saturated porous solid. II. Higher frequency range. *Journal of the Acoustical Society of America*, *28*(2), 179–191. https://doi.org/10.1121/1.1908241

Broglia, C., & Ellis, D. (1990). Effect of alteration, formation absorption, and standoff on the response of the thermal neutron porosity log in Gabbros and basalts: Examples from deep sea drilling project-ocean drilling program sites. *Journal of Geophysical Research*, *95*(B6), 9171–9188. https://doi.org/10.1029/JB095iB06p09171

Brož, P., Bernhardt, H., Conway, S. J., & Parekh, R. (2021). An overview of explosive volcanism on Mars. *Journal of Volcanology and Geothermal Research*, *409*, 107125. https://doi.org/10.1016/j.jvolgeores.2020.107125

Buckingham, M. J. (2000). Wave propagation, stress relaxation, and grain-to-grain shearing in saturated, unconsolidated marine sediments. *Journal of the Acoustical Society of America*, *108*(6), 2796–2815. https://doi.org/10.1121/1.1322018

Carr, M. H. (1979). Formation of Martian flood features by release of water from confined aquifers. *Journal of Geophysical Research*, *84*(B6), 2995–3007. https://doi.org/10.1029/JB084iB06p02995

Cashman, K. V., & Kauahikaua, J. P. (1997). Reevaluation of vesicle distributions in basaltic lava flows. *Geology*, *25*(5), 419–422. https://doi.org/10.1130/0091-7613(1997)025<0419:ROVDIB>2.3.CO;2

Clifford, S. (1986). Mars: Crustal pore volume, cryospheric depth, and the global occurrence of groundwater. In *Mars: Evolution of its climate and atmosphere* (Vol. *599*, p. 18).

Clifford, S. (1997). The origin of the Martian intercrater plains-The role of liquefaction from impact and tectonic-induced seismicity. In *Lunar and planetary science conference* (Vol. *28*, p. 241).

Davis, R., & Haltigin, T. (2021). International Mars ice mapper mission: The first human exploration reconnaissance mission to Mars. In *Lunar and planetary science conference* (p. 2614).

Day-Lewis, F. D., Singha, K., & Binley, A. M. (2005). Applying petrophysical models to radar travel time and electrical resistivity tomograms: Resolution-dependent limitations. *Journal of Geophysical Research*, *110*(B8), B08206. https://doi.org/10.1029/2004JB003569

Dou, S., Nakagawa, S., Dreger, D., & Ajo-Franklin, J. (2017). An effective-medium model for P-wave velocities of saturated, unconsolidated saline permafrost. *Geophysics*, *82*(3), EN33–EN50. https://doi.org/10.1190/geo2016-0474.1

Dundas, C. M., Mellon, M. T., Conway, S. J., Daubar, I. J., Williams, K. E., Ojha, L., et al. (2021). Widespread exposures of extensive clean shallow ice in the midlatitudes of Mars. *Journal of Geophysical Research: Planets*, *126*(3), e2020JE006617. https://doi.org/10.1029/2020JE006617

Dvorkin, J., & Nur, A. (1996). Elasticity of high-porosity sandstones: Theory for two North Sea data sets. *Geophysics*, *61*(5), 1363–1370. https://doi.org/10.1190/1.1444059

Franzson, H., Guðfinnsson, G., Helgadóttir, H., & Frolova, J. (2010). Porosity, density and chemical composition relationships in altered Icelandic hyaloclastites.

Fu, J., & Lin, W. (2018). Elastic constants and homogenized moduli of gypsum structure based on density functional theory. In *Advances in computer science and engineering* (Vol. *120*, pp. 390–395). https://doi.org/10.2991/ifeesm-17.2018.73

Gassmann, F. (1951). Uber die elastizitat poroser medien. *Vierteljahrsschrift der Naturforschenden Gesellschaft in Zürich*, *96*, 1–23.

Golombek, M., Grott, M., Kargl, G., Andrade, J., Marshall, J., Warner, N., et al. (2018). Geology and physical properties investigations by the InSight lander. *Space Science Reviews*, *214*(5), 1–52. https://doi.org/10.1007/s11214-018-0512-7

Golombek, M., Warner, N., Grant, J., Hauber, E., Ansan, V., Weitz, C., et al. (2020). Geology of the InSight landing site on Mars. *Nature Communications*, *11*(1), 1–11. https://doi.org/10.1038/s41467-020-14679-1

Hanna, J. C., & Phillips, R. J. (2005). Hydrological modeling of the Martian crust with application to the pressurization of aquifers. *Journal of Geophysical Research*, *110*(E1), E01004. https://doi.org/10.1029/2004JE002330

Hobiger, M., Hallo, M., Schmelzbach, C., Stähler, S., Fäh, D., Giardini, D., et al. (2021). The shallow structure of Mars at the InSight landing site from inversion of ambient vibrations. *Nature Communications*, *12*(1), 1–13. https://doi.org/10.1038/s41467-021-26957-7

Kalapodis, N., Kampas, G., & Ktenidou, O.-J. (2020). A review towards the design of extraterrestrial structures: From regolith to human outposts. *Acta Astronautica*, *175*, 540–569. https://doi.org/10.1016/j.actaastro.2020.05.038

Karl, D., Cannon, K. M., & Gurlo, A. (2021). Review of space resources processing for Mars missions: Martian simulants, regolith bonding concepts and additive manufacturing. *Open Ceramics*, *9*, 100216. https://doi.org/10.1016/j.oceram.2021.100216

Lewis, K. W., Peters, S., Gonter, K., Morrison, S., Schmerr, N., Vasavada, A. R., & Gabriel, T. (2019). A surface gravity traverse on Mars indicates low bedrock density at Gale crater. *Science*, *363*(6426), 535–537. https://doi.org/10.1126/science.aat0738

Li, J., Beghein, C., Wookey, J., Davis, P., Lognonné, P., Schimmel, M., et al. (2022). Evidence for crustal seismic anisotropy at the insight lander site. *Earth and Planetary Science Letters*, *593*, 117654. https://doi.org/10.1016/j.epsl.2022.117654

Liu, J., Li, H., Sun, L., Guo, Z., Harvey, J., Tang, Q., et al. (2021). In-situ resources for infrastructure construction on Mars: A review. *International Journal of Transportation Science and Technology*, *11*(1), 1–16. https://doi.org/10.1016/j.ijtst.2021.02.001

Lognonné, P., Banerdt, W., Pike, W., Giardini, D., Christensen, U., Garcia, R. F., et al. (2020). Constraints on the shallow elastic and anelastic structure of Mars from InSight seismic data. *Nature Geoscience*, *13*(3), 213–220. https://doi.org/10.1038/s41561-020-0536-y

MacKinnon, D. J., & Tanaka, K. L. (1989). The impacted Martian crust: Structure, hydrology, and some geologic implications. *Journal of Geophysical Research*, *94*(B12), 17359–17370. https://doi.org/10.1029/JB094iB12p17359

Majmudar, T. S., & Behringer, R. P. (2005). Contact force measurements and stress-induced anisotropy in granular materials. *Nature*, *435*(7045), 1079–1082. https://doi.org/10.1038/nature03805

Makse, H. A., Gland, N., Johnson, D. L., & Schwartz, L. (2004). Granular packings: Nonlinear elasticity, sound propagation, and collective relaxation dynamics. *Physical Review E*, *70*(6), 061302. https://doi.org/10.1103/PhysRevE.70.061302

Makse, H. A., Gland, N., Johnson, D. L., & Schwartz, L. M. (1999). Why effective medium theory fails in granular materials. *Physical Review Letters*, *83*(24), 5070–5073. https://doi.org/10.1103/PhysRevLett.83.5070

Manga, M., & Wright, V. (2021). No cryosphere-confined aquifer below InSight on Mars. *Geophysical Research Letters*, *48*(8), e2021GL093127. https://doi.org/10.1029/2021GL093127

Mindlin, R. D. (1949). Compliance of elastic bodies in contact. *American Society of Mechanical Engineers*, *16*(3), 259–268. https://doi.org/10.1115/1.4009973

19448007, 2022, 15, Downloaded from https://agupubs.onlinelibrary.wiley.com/doi/10.1029/2022GL099250 by University Of California, Wiley Online Library on [18/04/2025]. See the Terms and Conditions (https://onlinelibrary.wiley.com/terms-and-conditions) on Wiley Online Library for rules of use; OA articles are governed by the applicable Creative Commons License

Moitra, P., Horvath, D. G., & Andrews-Hanna, J. C. (2021). Investigating the roles of magmatic volatiles, ground ice and impact-triggering on a very recent and highly explosive volcanic eruption on Mars. *Earth and Planetary Science Letters*, *567*, 116986. https://doi.org/10.1016/j.epsl.2021.116986

Morgan, G. A., Putzig, N. E., Perry, M. R., Sizemore, H. G., Bramson, A. M., Petersen, E. I., et al. (2021). Availability of subsurface water-ice resources in the northern mid-latitudes of Mars. *Nature Astronomy*, *5*(3), 230–236. https://doi.org/10.1038/s41550-020-01290-z

Murphy, W. F. (1982). *Effects of microstructure and pore fluids on the acoustic properties of granular sedimentary materials (Unpublished doctoral dissertation)*. Stanford University.

Pan, L., Quantin-Nataf, C., Tauzin, B., Michaut, C., Golombek, M., Lognonné, P., et al. (2020). Crust stratigraphy and heterogeneities of the first kilometers at the dichotomy boundary in Western Elysium Planitia and implications for InSight lander. *Icarus*, *338*, 113511. https://doi.org/10.1016/j.icarus.2019.113511

Piqueux, S., Buz, J., Edwards, C. S., Bandfield, J. L., Kleinböhl, A., Kass, D. M., et al. (2019). Widespread shallow water ice on Mars at high latitudes and midlatitudes. *Geophysical Research Letters*, *46*(24), 14290–14298. https://doi.org/10.1029/2019GL083947

Rivera-Valentín, E. G., Chevrier, V. F., Soto, A., & Martínez, G. (2020). Distribution and habitability of (meta) stable brines on present-day Mars. *Nature Astronomy*, *4*(8), 756–761. https://doi.org/10.1038/s41550-020-1080-9

Scheller, E., Ehlmann, B., Hu, R., Adams, D., & Yung, Y. (2021). Long-term drying of Mars by sequestration of ocean-scale volumes of water in the crust. *Science*, *372*(6537), 56–62. https://doi.org/10.1126/science.abc7717

Sharma, S. S., & Fahey, M. (2003). Degradation of stiffness of cemented calcareous soil in cyclic triaxial tests. *Journal of Geotechnical and Geoenvironmental Engineering*, *129*(7), 619–629. https://doi.org/10.1061/(ASCE)1090-0241(2003)129:7(619)

Smrekar, S. E., Lognonné, P., Spohn, T., Banerdt, W. B., Breuer, D., Christensen, U., et al. (2019). Pre-mission InSights on the interior of Mars. *Space Science Reviews*, *215*(1), 1–72. https://doi.org/10.1007/s11214-018-0563-9

Spohn, T., Hudson, T. L., Witte, L., Wippermann, T., Wisniewski, L., Kedziora, B., et al. (2022). The InSight-HP3 mole on Mars: Lessons learned from attempts to penetrate to depth in the Martian soil. *Advances in Space Research*, *69*(8), 3140–3163. https://doi.org/10.1016/j.asr.2022.02.009

Squyres, S., Aharonson, O., Arvidson, R., Bell, J., Christensen, P., Clark, B., et al. (2006). Bedrock formation at meridiani planum. *Nature*, *443*(7107), E1–E2. https://doi.org/10.1038/nature05212

Squyres, S., Arvidson, J., Bell, J., Brückner, N., Cabrol, W., Calvin, M., et al. (2004). The opportunity rover's Athena science investigation at meridiani planum, Mars. *Science*, *306*(5702), 1698–1703. https://doi.org/10.1126/science.1106171

Suazo, G., Fourie, A., & Doherty, J. (2017). Cyclic shear response of cemented paste backfill. *Journal of Geotechnical and Geoenvironmental Engineering*, *143*(1), 04016082. https://doi.org/10.1061/(ASCE)GT.1943-5606.0001581

Sun, V. Z., Stack, K. M., Kah, L. C., Thompson, L., Fischer, W., Williams, A. J., et al. (2019). Late-stage diagenetic concretions in the Murray formation, Gale crater, Mars. *Icarus*, *321*, 866–890. https://doi.org/10.1016/j.icarus.2018.12.030

Suzuki, M., Umezaki, T., & Takahara, H. (2012). Fast and cyclic shearing of cemented sand in Earthquake induced landslide. In *Proceedings 15th world conference on earthquake engineering*.

Tanaka, K. L., Skinner, J. A., Jr., Dohm, J. M., Irwin, R. P., III, Kolb, E. J., Fortezzo, C. M., et al. (2014). Geologic map of Mars.

Vanorio, T., Prasad, M., & Nur, A. (2003). Elastic properties of dry clay mineral aggregates, suspensions and sandstones. *Geophysical Journal International*, *155*(1), 319–326. https://doi.org/10.1046/j.1365-246X.2003.02046.x

Walton, K. (1987). The effective elastic moduli of a random packing of spheres. *Journal of the Mechanics and Physics of Solids*, *35*(2), 213–226. https://doi.org/10.1016/0022-5096(87)90036-6

Wang, C.-Y., Manga, M., & Wong, A. (2005). Floods on Mars released from groundwater by impact. *Icarus*, *175*(2), 551–555. https://doi.org/10.1016/j.icarus.2004.12.003

Warner, N., Golombek, M., Ansan, V., Marteau, E., Williams, N., Grant, J., et al. (2022). In situ and orbital stratigraphic characterization of the InSight landing site—A type example of a regolith-covered lava plain on Mars. *Journal of Geophysical Research: Planets*, *127*(4), e2022JE007232. https://doi.org/10.1029/2022JE007232

Wernicke, L. J., & Jakosky, B. M. (2021). Martian hydrated minerals: A significant water sink. *Journal of Geophysical Research: Planets*, *126*(3), e2019JE006351. https://doi.org/10.1029/2019JE006351

Wright, V., & Hornbach, M. (2021). The effects of 180 years of aging on the physical and seismic properties of partially saturated sands. *Journal of Geophysical Research: Solid Earth*, *126*(6), e2020JB021341. https://doi.org/10.1029/2020JB021341

Zeghal, M., & El Shamy, U. (2008). Liquefaction of saturated loose and cemented granular soils. *Powder Technology*, *184*(2), 254–265. https://doi.org/10.1016/j.powtec.2007.11.032

Zimmer, M. A., Prasad, M., Mavko, G., & Nur, A. (2007). Seismic velocities of unconsolidated sands: Part 1—Pressure trends from 0.1 to 20 MPa. *Geophysics*, *72*(1), E1–E13. https://doi.org/10.1190/1.2399459

Zong, J., Stewart, R. R., Dyaur, N., & Myers, M. T. (2017). Elastic properties of rock salt: Laboratory measurements and Gulf of Mexico well-log analysis. *Geophysics*, *82*(5), D303–D317. https://doi.org/10.1190/geo2016-0527.1

References From the Supporting Information

Christensen, N. I. (1972). Compressional and shear wave velocities at pressures to 10 kilobars for basalts from the East Pacific Rise. *Geophysical Journal International*, *28*(5), 425–429. https://doi.org/10.1111/j.1365-246X.1972.tb06140.x

Mavko, G., Mukerji, T., & Dvorkin, J. (2020). *The rock physics handbook*. Cambridge university press.

Toksöz, M. N., Cheng, C., & Timur, A. (1976). Velocities of seismic waves in porous rocks. *Geophysics*, *41*(4), 621–645. https://doi.org/10.1190/1.1440639

Woeber, A., Katz, S., & Ahrens, T. (1963). Elasticity of selected rocks and minerals. *Geophysics*, *28*(4), 658–663. https://doi.org/10.1190/1.1439242

19448007, 2022, 15, Downloaded from https://agupubs.onlinelibrary.wiley.com/doi/10.1029/2022GL099250 by University Of California, Wiley Online Library on [18/04/2025]. See the Terms and Conditions (https://onlinelibrary.wiley.com/terms-and-conditions) on Wiley Online Library for rules of use; OA articles are governed by the applicable Creative Commons License